Memorias del XX Congreso Latinoamericano de Control Automático (CLCA 2025)
13-17 de Octubre, 2025. Cancún, Quintana Roo, México

Ultra-local Model Predictive Current Control of a PM Synchronous Motor

F. González Sáenz * **O. Sandre Hernández** **
C. Cuvas Castillo *** **J. P. Ordaz Oliver** *

* *CITIS, AACyE, ICBI, Autonomous University of Hidalgo State, Pachuca 42184, Hidalgo, Mexico; fbsaenz095@gmail.com*
** *SECIHTI-UAEH, CITIS, AACyE, ICBI, Autonomous University of Hidalgo State, Pachuca 42184, Hidalgo, Mexico; omar_sandre@uaeh.edu.mx*
*** *UPP, Polytechnic University of Pachuca, Zempoala 43830, Hidalgo, Mexico; carlos.cuvas@upp.edu.mx*

Abstract: This paper introduces an ultra-local model predictive current control (UMPCC) for a permanent magnet synchronous motor (PMSM). The main objective of the ultra-local model approach is to improve the robustness of the current control of the PMSM. Previous works on ultra-local model techniques for the current control of a PMSM are designed based on deadbeat control, which leads to a high current ripple due to the fast response of the controller. This paper introduces a continuous UMPCC (C-UMPCC) to minimize the current ripple. In the proposed approach, a continuous vector control is designed using the solution of an optimal control tracking problem. Simulation results are presented to illustrate the proposed controller.

Keywords: Kalman filter, PMSM, Predictive Current Control, Ultra-local Model

1. INTRODUCTION

The permanent magnet synchronous motor (PMSM) is widely used in industrial applications due to its compact size and high power density (Krishnan (2017)). Typically, field-oriented control (FOC) is used in servo drives for PMSM (Llorente (2020)). In FOC, the stator current and speed of the motor are controlled in a cascade loop using proportional-integral (PI) controllers. Since the PMSM is non-linear, the performance of the drive can be degraded with parameter changes or external disturbances when using PI controllers (Jia et al. (2019)).

To deal with the non-linear dynamics of the PMSM, model predictive control (MPC) has been widely used (Rodriguez et al. (2022)). In MPC, the PMSM model is used to predict the dynamic response of the current or the speed. Based on the response, the control action is obtained based on the minimization of a cost function. As the name implies, MPC is highly dependent on the mathematical model of the PMSM. Therefore, changes in machine parameters, external disturbances, or unmodeled dynamics will deteriorate the performance of the MPC (Zhang et al. (2023)).

To add robustness to internal (parameter variation) and external disturbances in PMSM control, the model-free MPC (MF-MPC) is an alternative to the conventional MPC (Wang et al. (2025)). MF-MPC is based on an ultra-local model where the internal and external disturbances are lumped. This results in a first-order system with an unknown term consisting of lumped disturbances (Fliess and Join (2013)). Hence, Ultra-local MPC (UL-MPC) results in an observer-based controller, where an extended state observer (ESO) is used to estimate the lumped disturbance, and then the control action is calculated based on this estimation.

Several works have been presented for the UL-MPC. In Liu et al. (2025), a MF-MPC for the current control of a PMSM is introduced. In this work, a modified ESO for harmonic disturbance suppression in combination with a deadbeat predictive current control (DPCC) is presented. In Li et al. (2023), a finite control set MPC (FCS-MPC) for the current control of a PMSM is introduced. In there, a Kalman filter is used to estimate the lumped disturbance using an augmented system model. In Mousavi et al. (2022), a FCS-MPC for the current control of an induction motor is proposed. In this work, the estimation of the lumped disturbance is based on an integral sliding mode observer. In Davari et al. (2024), the Kalman filter is used as a compensation for the measurement error for the MF predictive current control of an Induction Motor. In this manuscript, the Kalman filter is used as a disturbance observer (DOB) using an ultra-local model. In Zhang et al. (2021), an ESO based on an ultra-local model for the predictive current control of a PMSM is introduced. In this work, a deadbeat control is formulated for the stator current regulation of the PMSM.

⋆ The authors thank the Ministry of Science, Humanities, Technology and Innovation (SECIHTI), Mexico, for the doctoral scholarship given to the first author of this paper, No. 4005734.

https://doi.org/10.58571/CNCA.AMCA.2025.008

In this paper, a robust ultra-local model predictive current control (UMPCC) for a PMSM is presented. The proposed method uses the Kalman filter as a DOB for the estimation of the lumped disturbance in the current loop. Then, the estimated disturbance is used to formulate a continuous UMPCC (C-UMPCC). The solution of the proposed C-UMPCC is obtained using a batch approach, which results in the optimal voltage control to be applied in the PMSM. This results in a lower current ripple of the machine in comparison with previous methods. Simulation results are presented to illustrate the proposed methodology.

2. CONVENTIONAL ESO-BASED UMPCC

2.1 PMSM mathematical model and Conventional DPCC

In this paper, a surface PMSM is considered. In the $d-q$ reference frame, the dynamics of the speed and current of the PMSM are given by Krishnan (2017):

$$\frac{d}{dt}\omega_m = \frac{1}{J}\left(M_e - M_L\right) \tag{1}$$
$$M_e = \frac{3}{2}p\psi_f i_{sq} \tag{2}$$
$$\frac{d}{dt}i_d = -\frac{R_s}{L_s}i_d + \omega_e i_q + \frac{1}{L_s}u_d, \tag{3}$$
$$\frac{d}{dt}i_q = -\frac{R_s}{L_s}i_q - \omega_e i_d - \frac{\omega_e\psi_f}{L_s} + \frac{1}{L_s}u_q, \tag{4}$$

where J is the rotor inertia, $M_{e,L}$ is electromagnetic torque and the load torque respectively, p is the pair poles, $i_{d,q}$ and $u_{d,q}$ are the stator currents and voltages respectively, R_s and L_s are the stator resistance and inductance respectively, ω_e is the electrical speed, ω_m is the mechanical speed, and ψ_f is the flux linkage of the permanent magnets of the rotor. Since MPC is formulated in the discrete-time domain, the continuous-time model of the PMSM is discretized based on the Euler method; hence, the discrete mathematical model of the dynamics of the current of the PMSM is given by:

$$i_{d_{k+1}} = \left(1 - T_s\frac{R_s}{L_s}\right)i_{d_k} + T_s\left(\omega_{e_k}i_{q_k} + \frac{1}{L_s}u_{d_k}\right), \tag{5}$$
$$i_{q_{k+1}} = \left(1 - T_s\frac{R_s}{L_s}\right)i_{q_k} + T_s\left(-\omega_{e_k}i_{d_k} - \frac{\omega_{e_k}\psi_f}{L_s} + \frac{1}{L_s}u_{q_k}\right), \tag{6}$$

where T_s is the sampling time, and the subindex k denotes the time step. For the system (5)-(6), the reference voltage vector of conventional DPCC can be obtained following a deadbeat control approach and is given by Liu et al. (2025):

$$u_{d_k} = \frac{L_s}{T_s}\left[i_d^* - \left(1 - T_s\frac{R_s}{L_s}\right)i_{d_k} - T_s\omega_{e_k}i_{q_k}\right], \tag{7}$$
$$u_{q_k} = \frac{L_s}{T_s}\left[i_q^* - \left(1 - T_s\frac{R_s}{L_s}\right)i_{q_k} - T_s\left(\omega_{e_k}i_{d_k} - \frac{\omega_{e_k}\psi_f}{L_s}\right)\right], \tag{8}$$

where $i_{d,q}^*$ are the reference currents.

2.2 Conventional ESO-Based MFPCC

Conventional DPCC requires accurate information about the PMSM parameters for appropriate operation. Under parameter mismatch, the current prediction is affected, resulting in a current tracking error and deterioration of the dynamic performance. An ultra-local model is used to add robustness against parameter variations. Then, the ultra-local model of the current dynamics of the PMSM is given by Zhang et al. (2021); Liu et al. (2025):

$$\frac{d}{dt}i_d = b_d u_d + f_d, \tag{9}$$
$$\frac{d}{dt}i_q = b_q u_q + f_q, \tag{10}$$

where $b_{d,q}$ are the control gains respectively, and can be selected as $b_d = b_q = 1/L_s$; $f_{d,q}$ are $d-q$ lumped disturbances respectively. $f_{d,q}$ can be written as:

$$f_d = -\frac{R_s}{L_s}i_d + \omega_e i_q + f_d', \tag{11}$$
$$f_q = -\frac{R_s}{L_s}i_q + \omega_e i_d - \frac{\omega_e\psi_f}{L_s} + f_q', \tag{12}$$

where $f_{d,q}'$ are the unmodeled disturbances of the system. The lumped disturbance in (9) - (10) is unknown but can be estimated using a DOB. For the system (9) - (10), the ESO is given by Zhang et al. (2021):

$$\begin{aligned}
\frac{d}{dt}\hat{i}_d &= b_d u_d + \hat{f}_d + \beta_1\left(i_d - \hat{i}_d\right),\\
\frac{d}{dt}\hat{i}_q &= b_q u_q + \hat{f}_q + \beta_1\left(i_q - \hat{i}_q\right),\\
\frac{d}{dt}\hat{f}_d &= \beta_2\left(i_d - \hat{i}_d\right),\\
\frac{d}{dt}\hat{f}_q &= \beta_2\left(i_q - \hat{i}_q\right),
\end{aligned} \tag{13}$$

where $\hat{i}_{d,q}$ and $\hat{f}_{d,q}$ are the estimation of current and lumped disturbance, respectively; $\beta_{1,2}$ are the feedback gains of the observer and can be selected as $\beta_1 = 2\omega_0$ and $\beta_2 = \omega_0^2$, where ω_0 is the bandwidth of the ESO. ω_0 can be selected according to pole location as in Zhang et al. (2021).

The conventional ESO-Based MFPCC is based on the ultra-local model of the PMSM and the ESO, hence, the discrete-time approximation of (9) and (10) is obtained using the Euler method:

$$i_{d_{k+1}} = i_{d_k} + T_s\left(b_d u_{d_k} + f_{d_k}\right), \tag{14}$$
$$i_{q_{k+1}} = i_{q_k} + T_s\left(b_q u_{q_k} + f_{q_k}\right). \tag{15}$$

Similarly, the discrete-time approximation of the ESO given by (13) is given by:

$$\hat{i}_{d_{k+1}} = \hat{i}_{d_k} + T_s\left[b_d u_{d_k} + \hat{f}_{d_k} + \beta_1\left(i_{d_k} - \hat{i}_{d_k}\right)\right], \tag{16}$$
$$\hat{i}_{q_{k+1}} = \hat{i}_{q_k} + T_s\left[b_q u_{q_k} + \hat{f}_{q_k} + \beta_1\left(i_{q_k} - \hat{i}_{q_k}\right)\right], \tag{17}$$
$$\hat{f}_{d_{k+1}} = \hat{f}_{d_k} + T_s\beta_2\left(i_{d_k} - \hat{i}_{d_k}\right), \tag{18}$$
$$\hat{f}_{q_{k+1}} = \hat{f}_{q_k} + T_s\beta_2\left(i_{q_k} - \hat{i}_{q_k}\right). \tag{19}$$

Finally, the reference voltage vector is obtained using the estimated disturbance and the deadbeat principle used in (7) and (8) as:

$$u_{d_k} = \frac{1}{T_s b_d}\left[i_d^* - i_{d_k} - T_s\hat{f}_{d_k}\right], \tag{20}$$
$$u_{q_k} = \frac{1}{T_s b_q}\left[i_q^* - i_{q_k} - T_s\hat{f}_{q_k}\right]. \tag{21}$$

 https://doi.org/10.58571/CNCA.AMCA.2025.008

Note that the settling time in deadbeat control depends on the sampling time. Small sampling times lead to a small settling time at the expense of a high control signal. Therefore, special attention must be paid to limit the control action within the operating voltage of the PMSM used.

3. CONTINUOUS UMPCC

An alternative to design the control action using the ultra-local PMSM model is to use a continuous MPC. Rather than using a single-step prediction, in C-UMPCC, a prediction is performed over a finite horizon, and a trajectory control is designed. The main advantage of the C-UMPCC is that the response of the control action is tuned by a weighting factor in the cost function. The proposed control is discussed in the following sections.

3.1 DOB-Based Kalman filter

One of the problems with linear observers like those introduced in Liu et al. (2025); Zhang et al. (2021) is the sensitivity to measurement error and noise. Determining the feedback gains commonly results in a trade-off between convergence and sensitivity. As introduced in Davari et al. (2024), the Kalman filter can be used as a DOB. Using (14) and (15), the PMSM ultra-local model is rewritten as:

$$\begin{aligned} x_{k+1} &= Gx_k + Hu_k + B_{dd}d_k, \\ y_k &= Cx_k, \end{aligned} \tag{22}$$

where

$$C = G = \begin{bmatrix} 1 & 0 \\ 0 & 1 \end{bmatrix}, \quad H = \begin{bmatrix} T_s b_d & 0 \\ 0 & T_s b_q \end{bmatrix}, \quad B_{dd} = \begin{bmatrix} T_s & 0 \\ 0 & T_s \end{bmatrix},$$

$$x_k = \begin{bmatrix} i_{d_k} & i_{q_k} \end{bmatrix}^T, \quad u_k = \begin{bmatrix} u_{d_k} & u_{q_k} \end{bmatrix}^T, \quad d_k = \begin{bmatrix} f_{d_k} & f_{q_k} \end{bmatrix}^T.$$

To estimate the disturbances, the following augmented system is used Li et al. (2023):

$$\begin{aligned} \overbrace{\begin{bmatrix} x_{k+1} \\ d_{k+1} \end{bmatrix}}^{\bar{x}_{k+1}} &= \overbrace{\begin{bmatrix} G & B_{dd} \\ 0 & I \end{bmatrix}}^{A} \overbrace{\begin{bmatrix} x_k \\ d_k \end{bmatrix}}^{\bar{x}_k} + \overbrace{\begin{bmatrix} H \\ 0 \end{bmatrix}}^{B} u_k, \\ y_k &= \underbrace{\begin{bmatrix} C & 0 \end{bmatrix}}_{C_o} \begin{bmatrix} x_k \\ d_k \end{bmatrix}. \end{aligned} \tag{23}$$

Using (21), the computation procedure for the estimation of the disturbance based on the standard Kalman filter is given as follows (Simon (2006)):

Rewriting (21) in the standard form of the Kalman filter, and given the following system:

$$\begin{aligned} \bar{x}_k &= A_{k-1}\bar{x}_{k-1} + B_{k-1}u_{k-1} + w_{k-1}, \\ y_k &= C_{o_k}\bar{x}_k + v_k, \\ E\left(w_k w_j^T\right) &= Q_k\delta_{k-j}, \\ E\left(v_k v_j^T\right) &= R_k\delta_{k-j}, \\ E\left(w_k v_j^T\right) &= 0, \end{aligned} \tag{24}$$

$$\delta_{k-j} = \begin{cases} 1 & k = j \\ 0 & k \neq j, \end{cases}$$

with initial conditions described as:

$$\begin{aligned} \hat{\bar{x}}_0^+ &= E\left(\bar{x}_0\right), \\ P_0^+ &= E\left[\left(\bar{x}_0 - \hat{\bar{x}}_0^+\right)\left(\bar{x}_0 - \hat{\bar{x}}_0^+\right)^T\right]. \end{aligned} \tag{25}$$

For every $k = 1, 2, \cdots$ the computation procedure of the standard Kalman filter is given by:

$$\begin{aligned} P_k^- &= A_{k-1}P_{k-1}^+A_{k-1}^T + Q_{k-1}, \\ K_k &= P_k^- C_{o_k}^T\left(C_{o_k}P_k^-C_{o_k}^T + R_k\right)^{-1}, \\ \hat{\bar{x}}_k^- &= A_{k-1}\hat{\bar{x}}_{k-1}^+ + B_{k-1}u_{k-1}, \\ \hat{\bar{x}}_k^+ &= \hat{\bar{x}}_k^- + K_k\left(y_k - C_{o_k}\hat{\bar{x}}_k^-\right), \\ P_k^+ &= \left(I - K_kC_{o_k}\right)P_k^-\left(I - K_kC_{o_k}\right)^T + K_kR_kK_k^T. \end{aligned} \tag{26}$$

in (24)-(26), Q and P denote covariance matrices of the system and measurement noise, respectively; $\hat{\bar{x}}_k = [\hat{x}_k,\ \hat{d}_k]^T$ is the estimation of the extended state $\bar{x}_k$; $\hat{\bar{x}}_k^-, \hat{\bar{x}}_k^+$ are the a priori and a posteriori estimates of the extended state, respectively; P_k^-, P_k^+ are the a priori and posteriori covariances of the measurement noise, respectively; and K_k is the Kalman gain.

3.2 Continuous UMPCC design

The objective of the C-UMPCC is to design a trajectory control to solve a reference tracking problem. The idea behind this proposal is similar to that introduced in Li et al. (2023). We assume that the desired reference r_p and the estimated disturbance $\hat{d}_k$ are constant over a prediction of finite horizon N. Then, the current reference of the PMSM is given by:

$$R_p^T = \overbrace{\begin{bmatrix} I_2 & I_2 & \cdots & I_2 \end{bmatrix}}^{N} r_p, \qquad r_p = [i_d^*,\ i_q^*]^T, \tag{27}$$

Now, considering the reference vector and the estimation of the disturbance $\hat{d}_k$, the following optimal control problem is introduced:

$$\begin{aligned} J_j^\star\left(x_j\right) = \min_{U_j} & \sum_{k=j}^{N-1}\left(r - y_k\right)^T Q_o\left(r - y_k\right) + u_k^T R_o u_k \\ & \textit{subject to} \\ & x_j = x_k, \\ & x_{k+1} = Gx_k + Hu_k + B_{dd}d_k, \quad k = 0, ..., N-1 \\ & d_{k+1} = d_k, \\ & y_k = Cx_k, \end{aligned} \tag{28}$$

where $U_j = \begin{bmatrix} u_k^T & u_{k+1}^T & u_{k+2}^T & \cdots & u_{k+N-1}^T \end{bmatrix}^T$ is the decision vector containing all the future inputs. $Q_o = Q_o^T \geq 0$; $R_o = R_o^T > 0$; are weighting matrices of appropriate dimensions. $Q_o = Q_o^T \geq 0$; $R_o = R_o^T > 0$. Q_o is a matrix that penalizes deviation from the reference, R_o is a matrix that penalizes the control action. For long prediction horizons, small values in Q_o and R_o results in an under-penalized deviation of the tracking error and control effort over time. Moreover, special attention is needed to scale properly Q_o and R_o and avoid ill-conditioned matrices. The solution to the problem introduced can be obtained

 https://doi.org/10.58571/CNCA.AMCA.2025.008

by using the gradient. To this end, let us introduce the following variables:

$$Y = \begin{bmatrix} y_k \\ y_{k+1} \\ \vdots \\ y_{k+N} \end{bmatrix}, \quad S^y = \begin{bmatrix} C \\ CG \\ \vdots \\ CG^N \end{bmatrix}, \quad D_j = \begin{bmatrix} d_k \\ d_{k+1} \\ \vdots \\ d_{k+N-1} \end{bmatrix},$$

$$S^r = \begin{bmatrix} 0 & 0 & 0 & \cdots & 0 \\ CH & 0 & 0 & \cdots & 0 \\ CGH & CH & 0 & \cdots & 0 \\ \vdots & \vdots & \vdots & \ddots & \vdots \\ CG^{N-1}H & CG^{N-2}H & CG^{N-3}H & \cdots & CH \end{bmatrix},$$

$$S^d = \begin{bmatrix} 0 & 0 & 0 & \cdots & 0 \\ CB_{dd} & 0 & 0 & \cdots & 0 \\ CGB_{dd} & CB_{dd} & 0 & \cdots & 0 \\ \vdots & \vdots & \vdots & \ddots & \vdots \\ CG^{N-1}B_{dd} & CG^{N-2}B_{dd} & CG^{N-3}B_{dd} & \cdots & CB_{dd} \end{bmatrix},$$

$$\bar{Q} = \begin{bmatrix} Q_o & 0 & \cdots & 0 \\ 0 & Q_o & \cdots & 0 \\ \vdots & \vdots & \ddots & 0 \\ 0 & 0 & \cdots & Q_o \end{bmatrix}, \quad \bar{R} = \begin{bmatrix} R_o & 0 & \cdots & 0 \\ 0 & R_o & \cdots & 0 \\ \vdots & \vdots & \ddots & 0 \\ 0 & 0 & \cdots & R_o \end{bmatrix}.$$

By using these definitions, the minimum of the problem introduced in (26) is given by:

$$\begin{aligned} &\nabla_{U(j)} J_j\left(x_j\right) = \\ &\quad \left(R_p - S^y x_k - S^d D_j\right)^T \bar{Q}\left(R_p - S^y x_k - S^d D_j\right) \\ &\quad - 2U_j^T S^{rT} \bar{Q}\left(R_p - S^y x_k - S^d D_j\right) \\ &\quad + U_j^T \left(S^{rT} \bar{Q} S^r + \bar{R}\right) U_j = 0. \end{aligned} \tag{29}$$

Finally, the optimal trajectory control $U_j^\star$ is given by:

$$U_j^\star = \left(S^{rT} \overline{Q} S^r + \overline{R}\right)^{-1} S^{rT} \overline{Q}\left(R_p - S^y x_k - S^d D_j\right), \tag{30}$$

and using the principle of receding horizon control, the optimal control action $u_k^\star$ is:

$$u_k^\star = \overbrace{\left[\, I_2 \;\; 0_2 \;\; \cdots \;\; 0_2 \,\right]}^{N} U_j^\star. \tag{31}$$

4. SIMULATION RESULTS

To evaluate the performance of the proposed methodology, the simplified scheme of the proposed control shown in Fig. 1 is implemented in Matlab/Simulink. The PMSM used in the simulation is a Trinamic motor model QBL 4208-100-04-025. The parameters for the simulation of the motor are taken from the manual or estimated using Bobek (2013) and are listed in Table 1. As shown in Fig. 1, the speed of the motor is controlled using a PI control, then, using the output as the i_q^* reference, and by setting the $i_d^* = 0$, the ultra-local MPCC is calculated. The voltages obtained using the ultra-local MPCC are converted to a PWM signal through the SV-PWM. SV-PWM is used because it leads to the maximum utilization

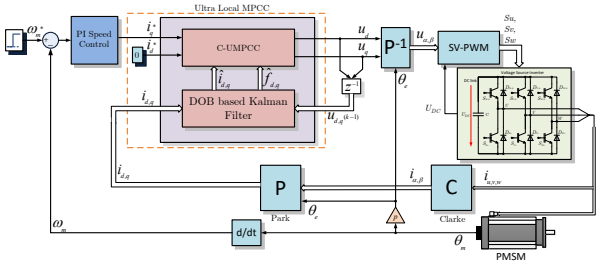

Fig. 1. Simplified block diagram of the C-UMPCC.

Table 1. Parameters of the PMSM

24V, 3-Φ, PMSM			
Parameter	**value**	**Parameter**	**value**
M_{LN}	0.25 Nm	p	4
R_s	0.1867 Ω	Ω_{nom}	4000 RPM
L_{sd}	0.36 mH	L_{sq}	0.36 mH
ψ_{PM}	0.006 Vs	i_N	6.95 A
J	$96 \cdot 10^{-6}$ kgm^2		

of the DC-link voltage and a reduced amount of current harmonics (Llorente (2020)).

The parameters used in the simulation are as follows: the solver chosen is 4th order Runge Kutta, the sampling time for the current loop is set to $T_s = 100\mu s$, and for the speed loop it is set to $T_s = 1ms$. Pole location is used for the PI gains of the speed loop, resulting in $Kp = 0.0824$ and $Ki = 0.000897$. The parameters of the Kalman filter are: $Q = \text{diag}(10, 10, 30e3, 30e3)$; $R = \text{diag}(10, 10)$, $P_0^+ = \text{diag}(1e5, 1e5, 1e5, 1e5)$. The parameters of the C-UMPCC are: $N = 10$, $Q_o = \text{diag}(8, 8)$ and $R_o = \text{diag}(0.2, 0.2)$. For the power inverter, a switching frequency of 20 kHz is used. For all simulations, the disturbances defined by (9) and (10) with $f'_{d,q} = 0$ are used as a reference for the Kalman filter estimation. A comparison with the control scheme introduced in Zhang et al. (2021) is presented. For this simulation, the bandwidth of the ESO ω_0 is selected as $\omega_0 = 300$ rad/s.

In the simulation, both controllers are set to follow the reference speed with a variable load torque. The speed reference is set to 100 rad/s at $t = 0.1s$, and at $t = 1.5s$ is set to -100 rad/s. The load torque is set as follows: in t=0s a $T_L = 0Nm$, in t=0.7s a $T_L = 0.25Nm$, in t=1.2s a $T_L = 0Nm$, in t=2.6s a $T_L = -0.25Nm$, and in t=3s a $T_L = -0.1Nm$. The reference value for the i_d current is set to zero. To simulate that a load is attached to the PMSM rotor, a rotor inertial load is added in simulations; hence, the rotor inertia load is set to $5J$.

The simulation results for the speed control are shown in Figs. 2 and 3 for the ESO-Based MFPCC and for the Kalman-Based C-UMPCC, respectively. The results show that the speed is successfully controlled despite the simulated rotor load on the shaft, which only leads to a larger settling time. Similarly, the disturbances caused by the load torque are mitigated in the speed response for both controllers. There is no significant difference in the speed response of both controllers, since the same speed controller is used and the current control does not affect the speed performance. In the current control, it can be

 https://doi.org/10.58571/CNCA.AMCA.2025.008

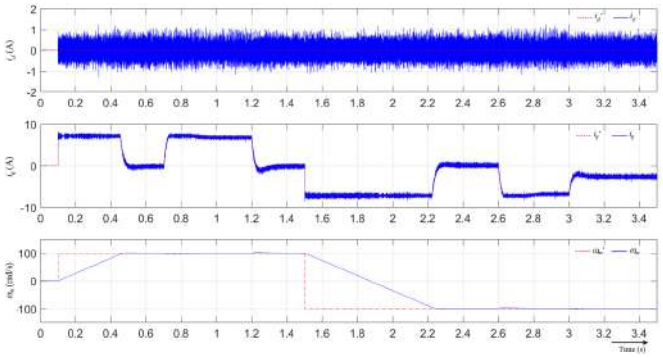

Fig. 2. ESO-Based DBMPC: controlled variables. From top: i_d current, i_q current, mechanical speed

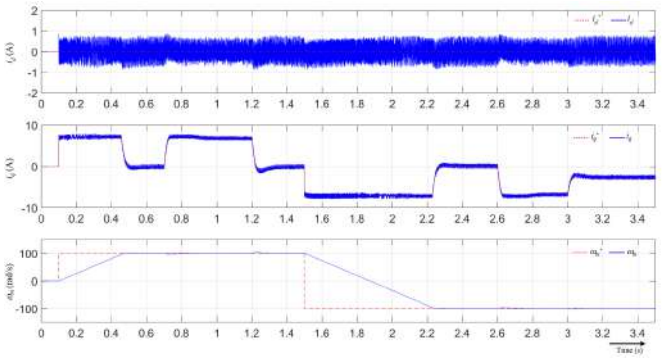

Fig. 3. Kalman-Based C-UMPCC: controlled variables. From top: i_d current, i_q current, mechanical speed

seen that the i_q current amplitude changes according to the the applied load torque. Furthermore, the Kalman-Based C-UMPCC results in lower current ripple in comparison with the ESO-Based MFPCC. Notice that the dynamic response is similar using the proposed Kalman-Based C-UMPCC compared to the ESO-Based MFPCC, and that the i_q current for the proposed Kalman-Based C-UMPCC is rapidly changed to mitigate the effect of disturbances on the speed response.

To evaluate the performance numerically, the root mean square error (RMSE) of the tracking is presented in Table 2. In this evaluation, the DOB-Based Kalman filter is combined with the MFPCC, and is referred to as Kalman-Based MFPCC. For current control, the best performance is obtained using the Kalman-Based C-UMPCC. It is important to note that when the MFPCC is used, a similar performance is obtained based on the ESO or the Kalman filter; therefore, a significant difference is not obtained when a difference observer is used. However, a better performance is obtained when the control is obtained based on the proposed approach.

The estimation of the variables of the extended state is shown in Fig. 4 and Fig. 5 for the ESO and the DOB-Based Kalman, respectively. It can be seen that the estimation of the currents is successfully obtained. In the ESO results, high noise is obtained for the current estimation. This noise may be caused by the noise introduced due to power electronics. For the DOB-based Kalman, a

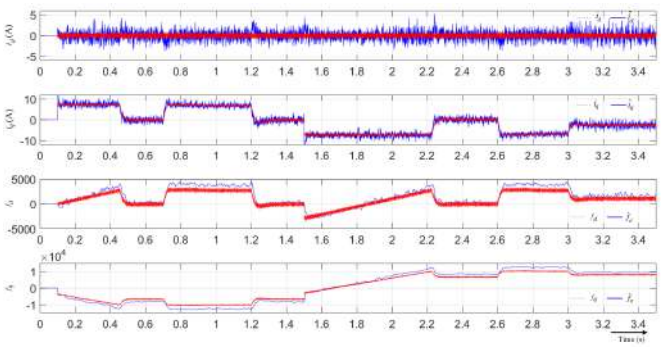

Fig. 4. DBMPC-ESO: observed variables. From top: i_d current, i_q current, f_d, f_q

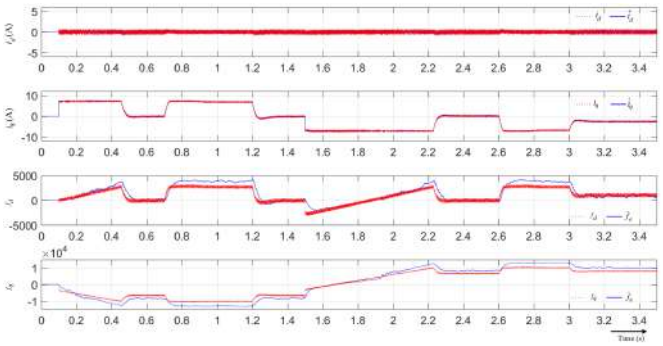

Fig. 5. C-UMPCC-Kalman DOB: observed variables. From top: i_d current, i_q current, f_d, f_q

Table 2. Evaluation of the RMSE tracking of the control schemes

Root Mean Square Error			
	ω_m	i_d	i_q
ESO-Based MFPCC	56.42959	0.36147	0.30176
Kalman-Based MFPCC	56.52009	0.36037	0.30362
Kalman-Based C-UMPCC	56.62802	0.30593	0.27759

Table 3. Evaluation of the RMSE estimation of the disturbance observers

Root Mean Square Error				
	$\hat{i}_d$	$\hat{i}_q$	$\hat{f}_d$	$\hat{f}_q$
ESO	0.9561	1.0391	761.3122	1711.2953
DOB-Based Kalman	0.1129	0.0993	728.0646	2049.3100

better performance is obtained in the current estimation. For the disturbance estimation, a similar performance is obtained for the ESO and the DOB-Based Kalman. A slightly higher ripple is observed in the ESO estimation. In both observers, a steady-state error is obtained for the disturbance estimation. This issue needs to be investigated further.

Finally, an evaluation of the RMSE estimation is presented in Table 3. The results show that the current estimation error is smaller for the DOB-Based Kalman in comparison with the ESO. In the case of the disturbance f_d, similar results are obtained for both observers; however, for the f_q disturbance, a smaller error is obtained for the ESO in comparison with the DOB-Based Kalman.

 https://doi.org/10.58571/CNCA.AMCA.2025.008

For both controllers, robustness of the current control depends upon the estimation of the disturbance; however, as shown in the simulation results, an estimation error leads to accurate performance of the drive. Mismatches in disturbance estimation will lead to a steady-state error in the system. Hence, for the proposed control scheme, an accurate estimator is needed. In the context of power electronics, the Kalman filter leads to a better estimation by considering the ripple introduced by the electronics commutation as noise; however, in this work, the statistics of the noise are unknown, and the Kalman filter parameters are designed by trial and error. Even though tuning the DOB-Based Kalman is time-consuming, the best results are obtained with its application in the proposed C-UMPCC.

The proposed C-UMPCC can be extended to other types of ac machines without requiring significant changes in its design. A drawback of the proposed control scheme is the computational cost introduced by the Kalman filter, in principle, the computational cost of the Kalman filter is more expensive in comparison with the ESO. In Simon (2006), an alternative formulation of the original Kalman filter is introduced to reduce the computational burden, however, when using this alternative formulation, special attention is needed to avoid divergence issues in the Kalman filter.

5. CONCLUSION

In this paper, a Kalman-based C-UMPCC is introduced. The proposed control scheme is based on the idea of active disturbance rejection control; hence, a DOB-Based Kalman estimator is used. The DOB-Based Kalman estimates the lumped disturbance of an ultra-local model for a PMSM drive, then the estimated disturbance is used in an optimal control problem to determine the optimal control action to be applied to the motor. In comparison with the previous work of ESO-Based MFPCC, the proposed control scheme results in lower current ripple in the machine. Despite the steady-state estimation error, the proposed methodology is capable of successfully control the currents of the machine. Future work is intended to increase the performance of the disturbance estimation and its application and verification in an experimental setup.

REFERENCES

Bobek, V. (2013). Pmsm electrical parameters measurement. *Freescale Semiconductor*, 7(8), 13.

Davari, S.A., Azadi, S., Flores-Bahamonde, F., Wang, F., Wheeler, P., and Rodriguez, J. (2024). Compensating the measurement error in model-free predictive control of induction motor via kalman filter-based ultra-local model. *IEEE Transactions on Power Electronics*, 39(12), 15811–15821. doi: 10.1109/TPEL.2024.3443134.

Fliess, M. and Join, C. (2013). Model-free control. *International Journal of Control*, 86(12), 2228–2252. doi:10.1080/00207179.2013.810345. URL `https://doi.org/10.1080/00207179.2013.810345`.

Jia, C., Wang, X., Liang, Y., and Zhou, K. (2019). Robust current controller for ipmsm drives based on explicit model predictive control with online disturbance observer. *IEEE Access*, 7, 45898–45910. doi: 10.1109/ACCESS.2019.2908383.

Krishnan, R. (2017). *Permanent magnet synchronous and brushless DC motor drives*. CRC press.

Li, X., Tian, W., Yang, Q., Karamanakos, P., and Kennel, R. (2023). Augmented multistep finite-control-set model predictive control for induction motor-drive system. *IEEE Transactions on Power Electronics*, 38(11), 13842–13854. doi:10.1109/TPEL.2023.3304950.

Liu, Z., Huang, X., Hu, Q., Yang, G., Wang, Y., and Shen, J. (2025). Model-free predictive current control of pmsm using modified extended state observer. *IEEE Transactions on Power Electronics*, 40(1), 679–690. doi:10.1109/TPEL.2024.3476318.

Llorente, R.M. (2020). *Practical control of electric machines: Model-based design and simulation*. Springer Nature.

Mousavi, M.S., Davari, S.A., Nekoukar, V., Garcia, C., and Rodriguez, J. (2022). Integral sliding mode observer-based ultralocal model for finite-set model predictive current control of induction motor. *IEEE Journal of Emerging and Selected Topics in Power Electronics*, 10(3), 2912–2922. doi: 10.1109/JESTPE.2021.3110797.

Rodriguez, J., Garcia, C., Mora, A., Davari, S.A., Rodas, J., Valencia, D.F., Elmorshedy, M., Wang, F., Zuo, K., Tarisciotti, L., Flores-Bahamonde, F., Xu, W., Zhang, Z., Zhang, Y., Norambuena, M., Emadi, A., Geyer, T., Kennel, R., Dragicevic, T., Khaburi, D.A., Zhang, Z., Abdelrahem, M., and Mijatovic, N. (2022). Latest advances of model predictive control in electrical drives—part ii: Applications and benchmarking with classical control methods. *IEEE Transactions on Power Electronics*, 37(5), 5047–5061. doi: 10.1109/TPEL.2021.3121589.

Simon, D. (2006). *Optimal state estimation: Kalman, H infinity, and nonlinear approaches*. John Wiley & Sons.

Wang, F., Wei, Y., Rodriguez, J., and Garcia, C. (2025). State-of-art, development, and challenges of model-free predictive control on motor drives. *IEEE Transactions on Power Electronics*, 40(8), 10846–10864. doi: 10.1109/TPEL.2025.3559514.

Zhang, Y., Jin, J., and Huang, L. (2021). Model-free predictive current control of pmsm drives based on extended state observer using ultralocal model. *IEEE Transactions on Industrial Electronics*, 68(2), 993–1003. doi:10.1109/TIE.2020.2970660.

Zhang, Y., Shen, W., and Yang, H. (2023). An improved deadbeat predictive current control of pmsm drives based on the ultra-local model. *Chinese Journal of Electrical Engineering*, 9(2), 27–37. doi: 10.23919/CJEE.2023.000020.

 https://doi.org/10.58571/CNCA.AMCA.2025.008